

# APPENDICES

|   |          |
|---|----------|
| Appendix A—Chemistry and water level data   | 5 pages  |
| Appendix B—Indications of surface water and shallow groundwater in the study area | 21 pages |
| Appendix C—Model description  | 3 pages  |
| Appendix D—Continuous water level measurements (on CD only)                       |          |



# APPENDIX A

## Chemistry and Water Level Data

| Code                                | Meaning                            | Unit               | Code              | Meaning                       | Unit            |
|-------------------------------------|------------------------------------|--------------------|-------------------|-------------------------------|-----------------|
| <sup>3</sup> H                      | Tritium                            | Tritium Units (TU) | Mo                | Molybdenum                    | mg/L            |
| <sup>3</sup> H: <sup>3</sup> He Age | Age of Water using dissolved gases | years              | Na                | Sodium                        | mg/L            |
| Ag                                  | Silver                             | mg/L               | Ni                | Nickel                        | mg/L            |
| Al                                  | Aluminum                           | mg/L               | NO <sub>2</sub>   | Nitrite (as NO <sub>2</sub> ) | mg/L            |
| As                                  | Arsenic                            | mg/L               | NO <sub>3</sub>   | Nitrate (as NO <sub>3</sub> ) | mg/L            |
| B                                   | Boron                              | mg/L               | δ <sup>18</sup> O | 18O:16O ratio                 | per mil (‰)     |
| Ba                                  | Barium                             | mg/L               | ORP               | Oxidation-Reduction Potential | mV              |
| Be                                  | Beryllium                          | mg/L               | Pb                | Lead                          | mg/L            |
| Br                                  | Bromide                            | mg/L               | pH Field          | pH, field                     | pH units        |
| δ <sup>13</sup> C                   | 13C:12C ratio                      | per mil (‰)        | PO <sub>4</sub>   | Phosphate                     | mg/L            |
| C <sup>14</sup>                     | 14C Apparent age (uncorrected)     | years              | Sb                | Antimony                      | mg/L            |
| Ca                                  | Calcium                            | mg/L               | Se                | Selenium                      | mg/L            |
| Cd                                  | Cadmium                            | mg/L               | Si                | Silicon                       | mg/L            |
| Cl                                  | Chloride                           | mg/L               | SiO <sub>2</sub>  | Silica                        | mg/L            |
| Co                                  | Cobalt                             | mg/L               | Sn                | Tin                           | mg/L            |
| Cond field                          | Specific Conductivity, field       | μs/cm              | SO <sub>4</sub>   | Sulfate                       | mg/L            |
| Cr                                  | Chromium                           | mg/L               | Sr                | Strontium                     | mg/L            |
| Cu                                  | Copper                             | mg/L               | Temp              | Temperature, field            | degrees celsius |
| DO                                  | Dissolved Oxygen, field            | mg/L               | TDS               | Total Dissolved Solids        | mg/L            |
| F                                   | Fluoride                           | mg/L               | Th                | Thorium                       | mg/L            |
| Fe                                  | Iron                               | mg/L               | Ti                | Titanium                      | mg/L            |
| δD                                  | Deuterium:Hydrogen ratio           | per mil (‰)        | Tl                | Thallium                      | mg/L            |
| HCO <sub>3</sub>                    | Bicarbonate                        | mg/L               | U                 | Uranium (total, by ICP-MS)    | mg/L            |
| HRD                                 | Hardness (CaCO <sub>3</sub> )      | mg/L               | V                 | Vanadium                      | mg/L            |
| K                                   | Potassium                          | mg/L               | Zn                | Zinc                          | mg/L            |
| Li                                  | Lithium                            | mg/L               | TAn               | Total anions                  | meq/L           |
| Mg                                  | Magnesium                          | mg/L               | TCat              | Total cations                 | meq/L           |
| Mn                                  | Manganese                          | mg/L               | IONBAL            | ion balance                   | % difference    |

**Table A1.** General chemistry data for well, and surface waters. Sample sites are shown on Figure 10.

| Site ID | NAD83<br>UTM<br>Easting | NAD83<br>UTM<br>Northing | Sample<br>point ID | Collection<br>date | Water Type                                 | Site<br>Type | <sup>3</sup> H<br>(TU) | Ag<br>(mg/L) | Al<br>(mg/L) | ALK<br>(mg/L) | As<br>(mg/L) | B<br>(mg/L) |
|---------|-------------------------|--------------------------|--------------------|--------------------|--|--------------|------------------------|--------------|--------------|---------------|--------------|-------------|
| JM-005  | 327722                  | 3640834                  | JM-005A            | 17-Oct-13          | Na-Mg-Ca-SO <sub>4</sub>                   | Well         |                        | <0.0025      | <0.0025      | 161           | <0.0025      | 0.9         |
| JM-006  | 327628                  | 3648143                  | JM-006A            | 17-Oct-13          | Na-Ca-Mg-SO <sub>4</sub> -Cl               | Well         |                        | <0.0025      | <0.0025      | 99            | <0.0025      | 0.9         |
| JM-007  | 331513                  | 3653290                  | JM-007A            | 17-Oct-13          | Na-Ca-Mg-SO <sub>4</sub> -Cl               | Well         |                        | <0.0025      | <0.0025      | 108           | <0.0025      | 0.9         |
| JM-008  | 324827                  | 3652693                  | JM-008A            | 17-Oct-13          | Na-SO <sub>4</sub> -Cl                     | Well         | -0.1                   | <0.0025      | <0.0025      | 126           | 0.0042       | 0.8         |
| JM-035  | 297507                  | 3660425                  | JM-035A            | 16-Oct-13          | Na-SO <sub>4</sub> -HCO <sub>3</sub>       | Well         |                        | <0.0025      | <0.0025      | 312           | <0.0025      | 0.2         |
| JM-037  | 309033                  | 3658022                  | JM-037A            | 23-Oct-13          | Ca-Na-Mg-SO <sub>4</sub> -HCO <sub>3</sub> | Well         |                        | <0.0025      | <0.0025      | 272           | <0.0025      | 0.2         |
| JM-038  | 306216                  | 3654061                  | JM-038A            | 18-Oct-13          | Na-Ca-Mg-SO <sub>4</sub> -HCO <sub>3</sub> | Well         | 3.2                    | <0.0025      | <0.0025      | 283           | <0.0025      | 0.5         |
| JM-039  | 310661                  | 3652987                  | JM-039A            | 18-Oct-13          | Na-Ca-Mg-HCO <sub>3</sub> -SO <sub>4</sub> | Well         |                        | <0.0025      | 0.0088       | 253           | <0.0025      | 0.3         |
| JM-041  | 309159                  | 3647472                  | JM-041A            | 18-Oct-13          | Na-SO <sub>4</sub> -Cl                     | Well         | 0.0                    | <0.0025      | <0.0025      | 249           | <0.0025      | 0.5         |
| JM-042  | 307198                  | 3649247                  | JM-042A            | 18-Oct-13          | Na-Ca-HCO <sub>3</sub> -SO <sub>4</sub>    | Well         |                        | <0.0025      | <0.0025      | 309           | <0.0025      | 0.5         |
| JM-044  | 308701                  | 3634398                  | JM-044A            | 23-Oct-13          | Na-Mg-SO <sub>4</sub> -HCO <sub>3</sub>    | Well         |                        | <0.0025      | <0.0025      | 294           | 0.0042       | 1.3         |
| JM-054  | 313070                  | 3652465                  | JM-054A            | 16-Oct-13          | Ca-Na-Mg-HCO <sub>3</sub> -SO <sub>4</sub> | Well         | 4.1                    | <0.0025      | <0.0025      | 220           | <0.0025      | 0.1         |
| JM-058  | 311517                  | 3625631                  | JM-058A            | 23-Oct-13          | Na-Ca-SO <sub>4</sub> -Cl                  | Well         |                        | <0.0025      | <0.0025      | 82            | 0.0051       | 0.8         |
| JM-059  | 296489                  | 3653186                  | JM-059A            | 24-Oct-13          | Mg-Ca-HCO <sub>3</sub>                     | Well         | 3.4                    | <0.0005      | 0.0016       | 279           | 0.006        | 0.08        |
| JM-500  | 295452                  | 3666275                  | JM-500A            | 16-Oct-13          | Ca-Na-HCO <sub>3</sub> -SO <sub>4</sub>    | Spring       |                        | <0.0025      | <0.0025      | 271           | <0.0025      | 0.1         |
| JM-501  | 310516                  | 3663366                  | JM-501A            | 17-Oct-13          | Ca-HCO <sub>3</sub>                        | Playa        |                        | <0.0025      | 4.97         | 140           | 0.005        | 0.05        |
| JM-501  | 310516                  | 3663366                  | JM-501B            | 25-Mar-14          |  | Playa        |                        |              |              |               |              |             |
| JM-502  | 309551                  | 3672347                  | JM-502A            | 17-Oct-13          | Ca-HCO <sub>3</sub>                        | Playa        |                        | <0.0005      | 0.219        | 97            | 0.003        | 0.02        |
| JM-503  | 312413                  | 3652920                  | JM-503A            | 18-Oct-13          | Ca-SO <sub>4</sub>                         | Seep         | 3.2                    | <0.0025      | 1.33         | 166           | <0.0025      | 0.09        |
| JM-503  | 312413                  | 3652920                  | JM-503B            | 26-Mar-14          |  | Seep         |                        |              |              |               |              |             |
| JM-504  | 301489                  | 3674351                  | JM-504A            | 04-Nov-13          | Na-HCO <sub>3</sub> -SO <sub>4</sub>       | Spring       | 0.1                    | <0.0005      | 0.006        | 345           | 0.0008       | 0.4         |
| JM-506  | 312608                  | 3652893                  | JM-506A            | 26-Mar-14          |  | Seep         |                        |              |              |               |              |             |
| JM-507  | 312964                  | 3649428                  | JM-507A            | 25-Mar-14          |  | Seep         |                        |              |              |               |              |             |
| JM-508  | 303708                  | 3672038                  | JM-508A            | 27-Mar-14          |  | Spring       |                        |              |              |               |              |             |

Table A1—Continued

[illegible]

Table A1—Continued

[illegible]

Table A1—Continued

[illegible]

Table A1—Continued

| Site ID | Site Type | TI (mg/L) | U (mg/L) | V (mg/L) | Zn (mg/L) | TAn (meq/L) | TCat (meq/L) | IONBAL (%) |
|---------|-----------|-----------|----------|----------|-----------|-------------|--------------|------------|
| JM-005  | Well      | <0.0025   | 0.02     | 0.01     | 0.02      | 21.4        | 20.3         | -2.8       |
| JM-006  | Well      | <0.0025   | 0.02     | 0.01     | 0.02      | 22.7        | 22.1         | -1.2       |
| JM-007  | Well      | <0.0025   | 0.01     | 0.01     | 0.0048    | 27.6        | 26.2         | -2.8       |
| JM-008  | Well      | <0.0025   | 0.02     | 0.03     | 0.0353    | 14.2        | 13.5         | -2.6       |
| JM-035  | Well      | <0.0025   | <0.0025  | <0.0025  | 1.23      | 18.0        | 17.1         | -2.6       |
| JM-037  | Well      | <0.0025   | 0.007    | <0.0025  | 0.02      | 16.1        | 15.5         | -1.8       |
| JM-038  | Well      | <0.0025   | 0.010    | <0.0025  | 0.0094    | 14.9        | 14.7         | -0.9       |
| JM-039  | Well      | <0.0025   | 0.007    | <0.0025  | 0.0072    | 9.7         | 9.7          | -0.3       |
| JM-041  | Well      | <0.0025   | 0.003    | <0.0025  | 0.0086    | 29.4        | 27.7         | -3.0       |
| JM-042  | Well      | <0.0025   | 0.0041   | <0.0025  | 0.0045    | 10.4        | 10.2         | -1.3       |
| JM-044  | Well      | <0.0025   | 0.04     | 0.05     | 0.09      | 27.3        | 26.4         | -1.7       |
| JM-054  | Well      | <0.0025   | 0.005    | 0.00     | 0.04      | 6.4         | 6.3          | -0.8       |
| JM-058  | Well      | <0.0025   | 0.008    | 0.03     | 0.01      | 28.9        | 27.4         | -2.6       |
| JM-059  | Well      | <0.0005   | 0.002    | 0.03     | 1.9       | 6.4         | 6.4          | -0.1       |
| JM-500  | Spring    | <0.0025   | <0.0025  | <0.0025  | 0.0164    | 11.4        | 11.4         | -0.3       |
| JM-501  | Playa     | <0.0025   | <0.0025  | 0.02     | 0.0092    | 3.0         | 3.2          | 2.7        |
| JM-501  | Playa     |           |          |          |           |             |              |            |
| JM-502  | Playa     | <0.0005   | <0.0005  | 0.01     | 0.0018    | 2.2         | 2.2          | 0.6        |
| JM-503  | Seep      | <0.0025   | 0.005    | 0.00     | 0.0034    | 17.4        | 17.1         | -0.9       |
| JM-503  | Seep      |           |          |          |           |             |              |            |
| JM-504  | Spring    | <0.0005   | 0.0006   | 0.0005   | 0.0022    | 12.1        | 11.7         | -1.8       |
| JM-506  | Seep      |           |          |          |           |             |              |            |
| JM-507  | Seep      |           |          |          |           |             |              |            |
| JM-508  | Spring    |           |          |          |           |             |              |            |

Table A2. Water level measurements.

| Site ID | NAD83 UTM<br>Easting | NAD83 UTM<br>Northing | Elevation<br>(ft above sea level) | Well depth<br>(ft below ground surface) | Date<br>measured | Depth to water<br>(ft below ground surface) |
|---------|----------------------|-----------------------|-----------------------------------|---|------------------|---|
| JM-001  | 319283               | 3645249               | 4545                              | 325                                     | 12/5/2012        | 91.30                                       |
| JM-002  | 318396               | 3644997               | 4499                              | 200                                     | 12/5/2012        | 71.66                                       |
| JM-003  | 316205               | 3634489               | 4397                              | 405                                     | 12/5/2012        | 320.14                                      |
| JM-005  | 327722               | 3640834               | 4652                              | 335                                     | 12/5/2012        | 271.24                                      |
| JM-006  | 327628               | 3648143               | 4824                              | 450                                     | 12/5/2012        | 361.23                                      |
| JM-007  | 331513               | 3653290               | 5189                              | 500                                     | 12/6/2012        | 353.41                                      |
| JM-008  | 324827               | 3652693               | 4796                              | 390                                     | 12/6/2012        | 320.67                                      |
| JM-012  | 314718               | 3647895               | 4579                              | 220                                     | 1/24/2013        | 47.38                                       |
| JM-013  | 315266               | 3647787               | 4575                              | 340                                     | 1/24/2013        | 72.71                                       |
| JM-014  | 316071               | 3647688               | 4551                              | 160                                     | 1/24/2013        | 78.35                                       |
| JM-015  | 303497               | 3667536               | 4857                              | 362                                     | 5/16/2013        | 143.00                                      |
| JM-016  | 310158               | 3672371               | 4757                              | 160                                     | 5/16/2013        | 96.01                                       |
| JM-017  | 303509               | 3672087               | 4580                              | 150                                     | 5/16/2013        | 25.69                                       |
| JM-022  | 295159               | 3644428               | 5721                              | 500                                     | 5/24/2013        | 323.75                                      |
| JM-023  | 294734               | 3644741               | 5759                              | 400                                     | 5/24/2013        | 99.65                                       |
| JM-027  | 306977               | 3665051               | 4761                              |   | 5/13/2013        | 55.71                                       |
| JM-028  | 307941               | 3661502               | 4796                              | 200                                     | 5/13/2013        | 93.67                                       |
| JM-030  | 306131               | 3662558               | 4853                              | 1100                                    | 5/13/2013        | 88.41                                       |
| JM-031  | 302076               | 3662454               | 4937                              | 140                                     | 5/13/2013        | 121.62                                      |
| JM-032  | 303359               | 3658930               | 4906                              |   | 5/13/2013        | 65.75                                       |
| JM-033  | 301844               | 3656239               | 5070                              |   | 5/13/2013        | 118.85                                      |
| JM-035  | 297507               | 3660425               | 4926                              | 175                                     | 5/14/2013        | 50.83                                       |
| JM-037  | 309033               | 3658022               | 4774                              |   | 5/23/2013        | 39.39                                       |
| JM-038  | 306216               | 3654061               | 4813                              | 40                                      | 5/15/2013        | 17.70                                       |
| JM-039  | 310661               | 3652987               | 4705                              | 60                                      | 5/15/2013        | 25.90                                       |
| JM-040  | 310109               | 3650189               | 4692                              | 150                                     | 5/15/2013        | 121.32                                      |
| JM-041  | 309159               | 3647472               | 4735                              | 220                                     | 5/15/2013        | 202.76                                      |
| JM-042  | 307198               | 3649247               | 4791                              | 160                                     | 5/16/2013        | 53.38                                       |
| JM-043  | 304384               | 3666213               | 4829                              | 300                                     | 5/16/2013        | 64.82                                       |
| JM-044  | 308701               | 3634398               | 4518                              | 265                                     | 5/22/2013        | 66.56                                       |
| JM-045  | 312589               | 3640874               | 4568                              | 200                                     | 5/22/2013        | 137.33                                      |
| JM-046  | 306216               | 3640960               | 4737                              |   | 5/22/2013        | 101.01                                      |
| JM-047  | 304614               | 3639134               | 4763                              | 180                                     | 5/22/2013        | 129.96                                      |
| JM-048  | 312540               | 3640812               | 4571                              | 210                                     | 5/22/2013        | 139.33                                      |
| JM-049  | 301243               | 3650176               | 5135                              | 134                                     | 5/24/2013        | 111.55                                      |
| JM-052  | 295629               | 3648391               | 5610                              | 265                                     | 5/28/2013        | 179.14                                      |
| JM-053  | 313077               | 3652498               | 4653                              | 285                                     | 5/28/2013        | 90.17                                       |
| JM-054  | 313070               | 3652465               | 4652                              | 150                                     | 5/28/2013        | 89.96                                       |
| JM-059  | 296489               | 3653186               | 5387                              | 220                                     | 10/24/2013       | 129.31                                      |
| JM-045  | 312589               | 3640874               | 4568                              | 200                                     | 5/22/2013        | 137.33                                      |
| JM-045  | 312589               | 3640874               | 4568                              | 200                                     | 10/23/2013       | 137.33                                      |
| JM-046  | 306216               | 3640960               | 4737                              |   | 5/22/2013        | 101.01                                      |
| JM-046  | 306216               | 3640960               | 4737                              |   | 10/23/2013       | 101.01                                      |
| JM-047  | 304614               | 3639134               | 4763                              | 180                                     | 5/22/2013        | 129.96                                      |
| JM-047  | 304614               | 3639134               | 4763                              | 180                                     | 10/23/2013       | 130.64                                      |
| JM-048  | 312540               | 3640812               | 4571                              | 210                                     | 5/22/2013        | 139.33                                      |
| JM-048  | 312540               | 3640812               | 4571                              | 210                                     | 10/23/2013       | 139.36                                      |
| JM-049  | 301243               | 3650176               | 5135                              | 134                                     | 5/24/2013        | 111.55                                      |
| JM-052  | 295629               | 3648391               | 5610                              | 265                                     | 5/28/2013        | 179.14                                      |
| JM-052  | 295629               | 3648391               | 5610                              | 265                                     | 10/24/2013       | 158.30                                      |
| JM-053  | 313077               | 3652498               | 4653                              | 285                                     | 5/28/2013        | 90.17                                       |
| JM-053  | 313077               | 3652498               | 4653                              | 285                                     | 10/16/2013       | 61.03                                       |
| JM-054  | 313070               | 3652465               | 4652                              | 150                                     | 5/28/2013        | 89.96                                       |
| JM-054  | 313070               | 3652465               | 4652                              | 150                                     | 10/17/2013       | 23.02                                       |
| JM-059  | 296489               | 3653186               | 5387                              | 220                                     | 10/24/2013       | 129.31                                      |





## APPENDIX B

# Indications of Surface Water and Shallow Groundwater in the Study Area

Trevor Kludt, Dave Love, and Bruce Allen

### Introduction

As part of the effort to delineate landforms and to define the paleohydrology of the project area, field work was undertaken in the study area, from Engle in the north to Point of Rocks in the south. This appendix contains observations regarding the presence of surface water in the project area, as well as indications of shallow ground water.

Surface water was noted in a number of locations, including seeps, springs, and playa basins filled by recent monsoon rainfall. In a number of locations, the presence of evaporites, iron oxide staining, and/or magnesium coatings in arroyo sidewalls indicate the presence of shallow ground water at these locations sometime in the past. Organic staining in deposits exposed in arroyo sidewalls at a few locations suggests that wet meadows or cienegas may have existed in these locations. However, during field work, no direct evidence was found indicating the presence of

previously undocumented paleo-springs in the study area.

The following appendix is divided into three sections. The first section discusses the geochemical indicators of shallow ground water, particularly as they are manifest in the study area. This section provides necessary geochemical background information for the evaluation of shallow ground water traces noted by the authors across the study area. The second section documents locations within the study area where surface waters and shallow ground water are accessible in the present or have been in the recent past (A.D. 1600 to the present). The third section documents locations which show indications of shallow ground water in the more distant past (pre-dating A.D. 1600).

The more recent locations are designated ‘M’ for modern on the accompanying map, while the older locations are designated ‘P’ for past (Figure B1). This temporal distinction is intended to focus attention on indications of surface waters or shallow ground water during the time period in which El Camino Real was in use. It should be noted that no samples were

**Table B1.** A 1 Indicators of high water tables and other forms of wetlands.

| Criteria for Shallow Ground Water   | Figure No.   |
|---|--|
| Abundant indicator plants (e.g. salt grass, sedges, allenrolfia, phragmites, equisetum) | M-2, M-5, M-6, M-7, M-8, M-9, M-10, M-12, M-13   |
| Water loss due to phreatophytes (e.g. Saltcedar, willow, Cottonwood, Rabbitbrush)       | M-1, M-2, M-5, M-6, M-7, M-8, M-9, M-10, M-12, M-13                                    |
| Buildup of organic material   | M-6, M-7, M-8, M-9, M-10, M-12   |
| Buildup of minerals at or near the surface by groundwater contributions                 | M-2, M-7   |
| Evidence of mineral precipitation   | M-2, M-7, M-12, M-13, P-17, P-18, P-19, P-20, P-23, P-24, P-25, P-26, P-27, P-28, P-29 |
| Evidence of mineral alteration—by microbes or inorganically—Fe and Mn                   | P-17, P-18, P-19, P-20, P-28, P-29   |
| Criteria for other forms of wetland   |  |
| Accumulations of clays and precipitates in playas.                                      | M-14   |
| Accumulations of clay along low-gradient stream valleys.                                | M-14, P-21   |
| Shrink-swell clays with many scales of mud cracks and gilgai.                           | M-14   |

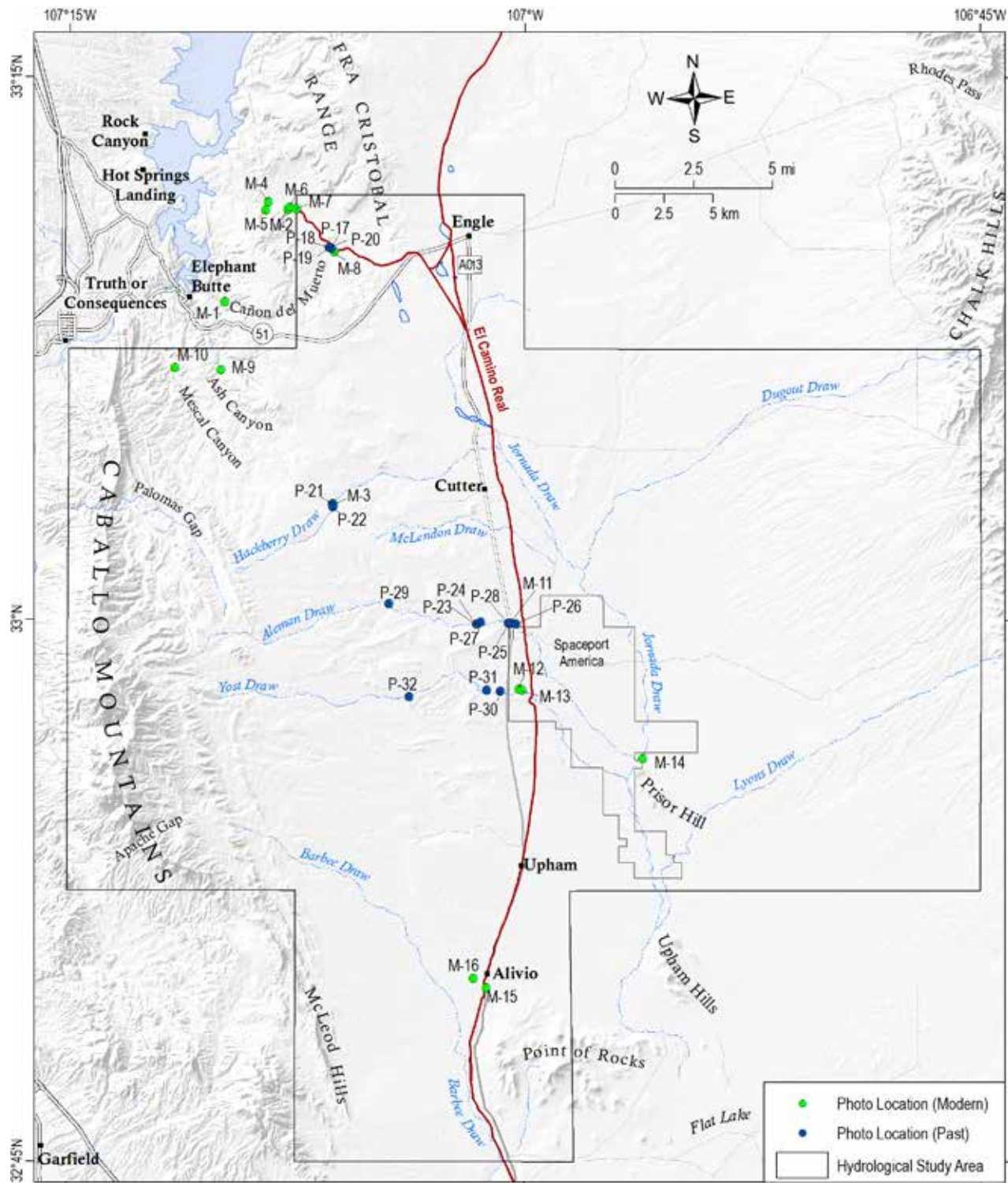


Figure B1. Surface water and shallow groundwater locations.

collected or processed to obtain radiometric ages, and that the ages presented here are estimates provided by the authors based on evident stratigraphic relationships, soil development, and/or previous experience.

For the most part, the locations discussed fall within the study area. Some are found outside of this boundary. The locations outside of this area have been included because they represent important regional water sources, or are illustrative of the numerous small scale springs/seeps found in the central portion of the study area.

## Primer on Geochemical Indicators of Past Groundwater Levels

**W**hat are indicators of groundwater levels past and present? Where groundwater presently intersects the land surface, one finds springs, seeps, bogs, wet meadows, riparian vegetation, and/or accumulations of tufa, travertine, or evaporite minerals such as gypsum or halite. These features depend on conditions of water discharge and chemistry, surface environment, and the length of time such conditions have existed. Springs and seeps along active arroyo channels may be short-lived, depending on recent stream-flow conditions and precipitation events upstream. Their presence may be indicated by animal excavations looking for water and by evaporite minerals at the surface. Commonly organic matter accumulates in wet meadows and marshes over many centuries to form dark brown or black soils. In semiarid environments, tufa or gypsum may accumulate as mounds at the surface relatively quickly. Evaporite minerals such as gypsum ( $\text{Ca}(\text{SO}_4)2\text{H}_2\text{O}$ ), other sulfate salts, or halite ( $\text{NaCl}$ ) may precipitate where water is evaporated at the surface. Evaporite minerals may also accumulate along the capillary fringe above the water table or at shallow depths as a separate soil horizon. Soluble evaporite minerals at the surface may form and dissolve again or blow away seasonally. Cementation of sediments in the shallow subsurface may take longer, requiring many pore-volumes of water passing through to accumulate enough minerals to coat and glue preexisting sedimentary grains or fracture faces. Common cements precipitated from groundwater include calcite ( $\text{CaCO}_3$ ), silica ( $\text{SiO}_2$ ), clays (complex fine-grained layered silicate minerals), iron oxides (hematite  $\text{Fe}_2\text{O}_3$ ; goethite,  $\alpha\text{-FeOOH}$ ), and manganese oxides (pyrolusite,  $\text{MnO}_2$ ).

Landscape features such as springs, wet meadows, tufa, and evaporate minerals were looked for along all major drainages in El Camino Real corridor.

Although springs and seeps are common locally, and wet meadows have formed locally down-gradient from Ojo del Muerto, evidence of past springs and wet meadows with dark boggy soils was not found. No evidence of tufa or travertine was found at the surface. Evidence of higher groundwater levels in the past are seen in alluvium along some of the present arroyos because their banks expose 3–5 m of deposits with varying amounts of precipitated minerals at various depths below the valley surface. These include bands of nodular calcite, crossbedded sandstones cemented with calcite, irregular masses and “fronts” of oxidized iron and manganese, and white powdery evaporite minerals (see following photo documentation). The summary of geochemical considerations presented below is meant to cover a few fundamentals that can be applied to observations along the corridor.

## Oxidation Potential and Acidity of Natural Waters

Water dissolves or alters many preexisting rocks and minerals that are in contact as it flows across the surface and in the subsurface. Water may also precipitate new minerals depending on local circumstances. Such processes are controlled by chemical laws of thermodynamics. Natural water has a range in the amount of oxygen in it (Eh, commonly called oxidation-reduction conditions) and a range in amounts of acids or bases (pH). These two properties largely control the types of reactions that take place and the resulting ions dissolved in the water. The ions in turn react with each other and with changing Eh-pH conditions within the water to precipitate minerals along its path. The following diagrams show calculated stability fields for inorganic reactions under equilibrium conditions and provide a sound basis for interpreting observed mineral precipitates. In nature, however, complications ensue as some reactions are not in equilibrium, but may be based on local kinetics and on presence of microbes that can take advantage of local conditions to use constituents in the water for their own nutrient and energy extraction and growth.

In nature, Eh affects colors of iron-bearing minerals. For example, reducing conditions (low Eh like bog water) causes iron in solution to have a +2 charge and color minerals like clays green or grayish green. Oxidizing conditions causes iron to have a +3 charge and become much less soluble so that iron minerals precipitate orange or red coatings on grains (see Figure B2).

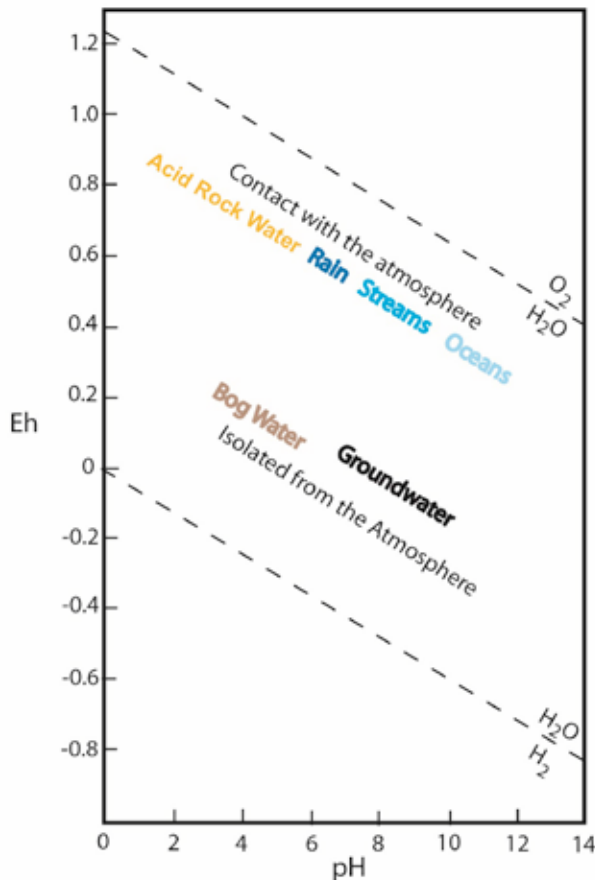


**Figure B2.** Diagram showing range of acid-base values (pH) and oxidation states (Eh) of natural waters at ordinary temperatures. The plot uses logarithmic increases for both pH and Eh. The upper and lower dashed diagonal lines indicate the upper and limits that water can exist at pH-Eh values. Diagram courtesy of Virgil Lueth.

### Iron and Manganese Coatings on Preexisting Grains

Iron and manganese are common in rock-forming minerals at and near the earth's surface. They both have different oxidation states depending on conditions of mineral formation and whether they have undergone weathering. As figures B3 to B5 show, in the presence of water, different ions and minerals are stable under different Eh-pH conditions.

### Dissolution and Precipitation of Calcium Carbonate

The mineral calcite (calcium carbonate;  $\text{CaCO}_3$ ) is a major rock-forming mineral in many environments and is a ubiquitous constituent of the land surface and dissolved in waters along the Jornada del Muerto. Thick limestone formations composed primarily of calcium carbonate are eroded from

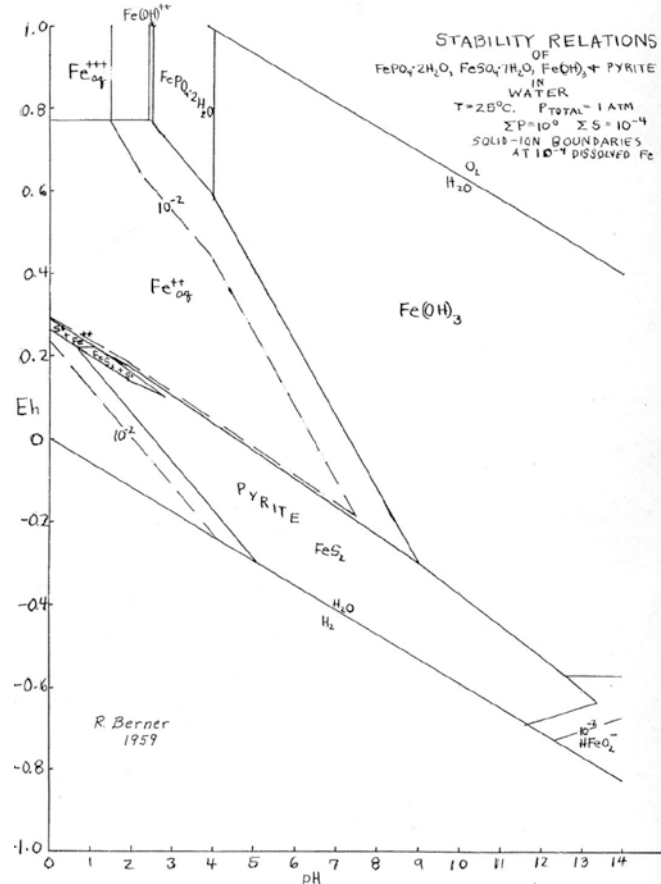
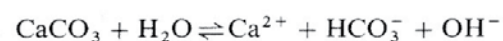


**Figure B3.** Eh-pH diagram of types of iron ions and solid phases (pyrite, vivianite) in system of water, sulfur, and phosphorous, calculated under equilibrium conditions (Berner, 1962b). This diagram is used to illustrate the iron ions in solution such as  $\text{Fe}^{2+}(\text{aq})$  and  $\text{Fe}(\text{OH})_3$ . Pyrite ( $\text{FeS}_2$ ) is the stable solid phase at low Eh over a range of pH values. The solid phosphosiderite ( $\text{Fe}(\text{PO}_4)_2\text{H}_2\text{O}$ ) only precipitates under low pH and high Eh conditions not seen in the study area.

surrounding the mountains to bring boulders, cobbles, pebbles, and finer grains to the piedmont slopes. Dust brings silt- and clay-sized calcite particles to surfaces of other deposits where rain dissolves and reprecipitates the carbonate in the shallow subsurface as a soil horizon or takes it down to the water table, where it travels with the water until conditions change and calcite precipitates again. In many instances, surface water and groundwater are nearly saturated with dissolved  $\text{CaCO}_3$ . The main chemical reactions of calcite in contact with water are the formation of calcium ions, various carbonate species, and hydroxyl ions.



If the system is in contact with the atmosphere containing carbon dioxide ( $\text{CO}_2$ ), that gas may either be

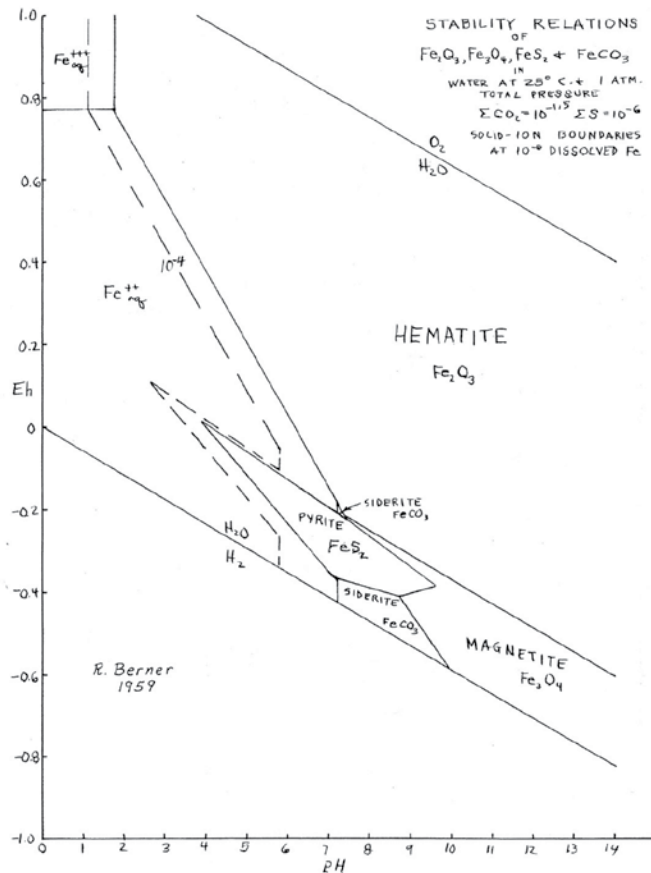
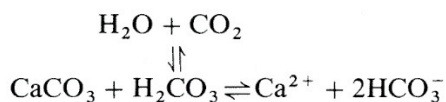


**Figure B4.** Eh-pH diagram showing dissolved ions of iron and solid phases in water also containing dissolved sulfur and carbon dioxide (Berner, 1962a). Note that hematite is the stable phase over the upper part of the Eh range for water. In nature, although hematite is common, a rust-colored hydrous mineral called goethite ( $\alpha\text{-FeOOH}$ ) and other hydrous iron phases are more common and are precursors to hematite. Also note that in the presence of dissolved  $\text{CO}_2$ , the field of pyrite stability is shrunk and siderite ( $\text{FeCO}_3$ ) and magnetite ( $\text{Fe}_3\text{O}_4$ ) are solids at low Eh and a range of high pH.

given off by the water or taken up by the water to change the amounts of various carbonate species:



This exchange depends on changes in temperature, pressure, organic activity, and decay of organic matter (Krauskopf, 1979). For example, if temperature rises,  $\text{CO}_2$  is given off by water, driving the equation to the left and precipitating calcite. If decay of organic matter produces acids, calcite is dissolved, moving the equation to the right.

The dominant carbonate species in solution depends on the pH of the water and dissolution of calcium carbonate can shift the pH to being more basic (pH greater than 7). See Figure B6.

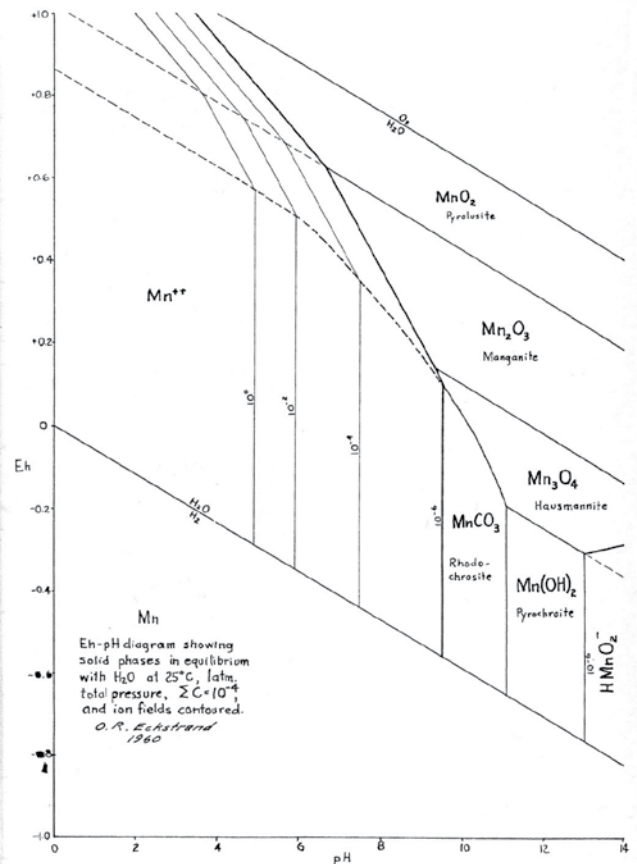


**Figure B5.** Eh-pH diagram showing dissolved ions of manganese and solid phases in water also containing dissolved carbon dioxide (Eckstrand, 1962). Note that under middle to low Eh conditions and pH below 9,  $\text{Mn}^{2+}$  ions remain dissolved. As waters become oxygenated (upward on diagram, and upward toward the surface of the water table), manganite and/or pyrolusite precipitate, forming black sooty coatings on preexisting grains of sediment.

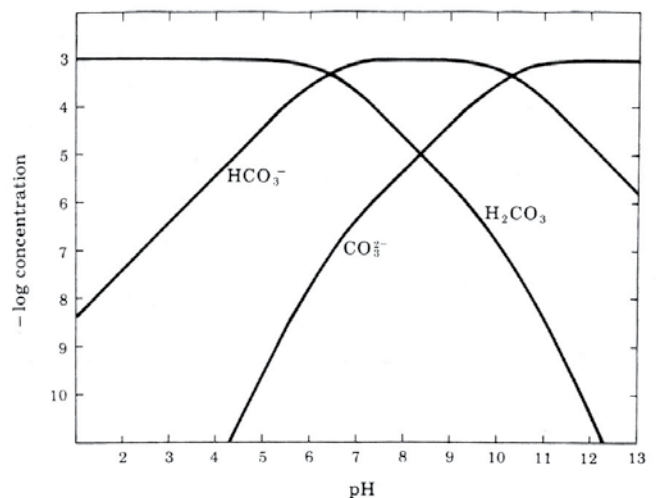


**Figure B6.** Diagram showing the concentrations of different dissolved carbonate species in water depending on pH of the system.  $\text{H}_2\text{CO}_3$  is carbonic acid, most abundant at pH < 6.  $\text{HCO}_3^-$  is the bicarbonate ion, most abundant between pH 6 and 11.  $\text{CO}_3^{2-}$  is most abundant in very basic solutions.



As mentioned above, calcium carbonate (commonly called caliche) builds up as a subsurface soil horizon 0.5–3 m below stable surfaces in semi-arid landscapes. The older surfaces have increased amounts of pedogenic (soil-generated) carbonate, designated with descriptors of stages from I (least) to VI (most). The stages IV through VI take millions of years to form. In stages II–VI, nodules of calcium carbonate can form in soils, but they also can form beneath water tables. Unfortunately the term “caliche” has also been applied to calcium carbonate precipitated along gullies—“gully bed caliche” or cementation. At some localities, it is difficult to determine whether the carbonate nodules are from soil-forming processes, from groundwater processes, or from both (Table B2 and Figure B6).

### Evaporite minerals at the capillary fringe

Some chemical constituents in water are more soluble than others and are less apt to come out of solution than others. When water is evaporated, these constituents may form “salts” or evaporite minerals (“evaporites”) which are combinations of cations such as  $\text{Ca}^{+2}$ ,  $\text{Na}^{+}$ ,  $\text{K}^{+}$ ,  $\text{Fe}^{+3}$ ,  $\text{Mg}^{+2}$ ,  $\text{Mn}^{+2}$ , and anions

such as  $\text{Cl}^{-}$ ,  $\text{SO}_4^{-2}$ ,  $\text{CO}_3^{-2}$ . The most common evaporites identified along the trail corridor are gypsum ( $\text{Ca}(\text{SO}_4)2\text{H}_2\text{O}$ ), halite ( $\text{NaCl}$ ), and thenardite ( $\text{Na}_2\text{SO}_4$ ).

**Table B2.** Stages of calcium carbonate accumulation in desert soils by Gile et al. (1981) and Monger et al. (2009).

| The stages of carbonate accumulation 1/  |   |   |
|--|---|---|
| Stage and general character  | Diagnostic carbonate morphology                       |   |
|  | Gravelly sequence                                     | Nongravelly sequence                      |
| I<br>Weakest expression of macroscopic carbonate   | Thin, discontinuous pebble coatings                   | Few filaments or faint coatings           |
| II<br>Carbonate segregations separated by low carbonate material   | Continuous pebble coatings, some interpebble fillings | Few to common nodules                     |
| III<br>Carbonate essentially continuous; plugged horizon forms in last part  | Many interpebble fillings                             | Many nodules and internodular fillings    |
| IV<br>Laminar horizon develops   | Laminar horizon overlying plugged horizon             | Laminar horizon overlying plugged horizon |
| V<br>Initial brecciation, recementation, and pisolith formation in the upper part of the laminar-plugged zone  |   |   |
| VI<br>Multiple generations of brecciation, recementation, and pisoliths are common. Stage VI horizons also have higher bulk densities and carbonate contents than do stages IV and V |   |   |

1/ The stages of carbonate accumulation follow Gile et al. (1966) and Birkeland et al. (1991). Pisoliths are subangular to spherical bodies, ranging from 2 mm to more than 10 mm in diameter, that have concentric coatings of carbonate around a nucleus that commonly consists of fragments of laminar and/or massive carbonate.

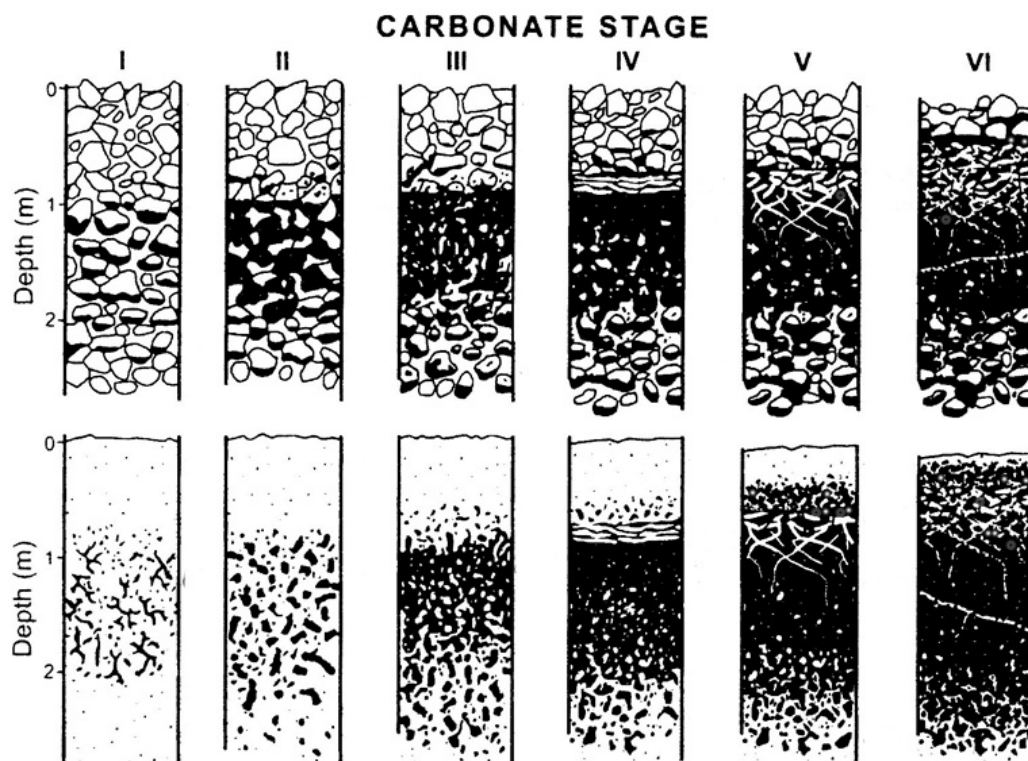


**Figure B6.** Stages of calcium carbonate accumulation in desert soils. Upper row, coarse parent material; lower row, fine-grained parent material (modified from a diagram by Bruce Harrison in Schaetzl and Anderson, 2005).

## Modern Surface Water and Shallow Groundwater Locations



**Figure M-1.** Unnamed spring, Jose Canyon. This spring is located just outside of project corridor, 3.6 miles southwest of Ojo del Muerto spring. The spring emerges in a gravel bed beneath the road. The spring comes up along a fault and is found in a syncline that funnels water toward the fault. No obvious spring deposits at the site, indicating that minerals in the water do not precipitate when reaching the atmosphere.



**Figure M-2.** McRae Canyon. Overlooking canyon to the northwest from hillside above present location of Ojo del Muerto spring. Note water in drainage channel and white evaporites on sandbars in arroyo. Historic Fort McRae located around curve above channel to left.



**Figure M-3.** Vertical dike. Dike (Ti; dark brownish gray under shovel) cutting gray, well cemented sandstone of the Cretaceous Crevasse Canyon Formation at Big Red Windmill, Hackberry Draw. No difference in cementation or flow of shallow subsurface water is observed at this dike. While there is no indication that this dike has obstructed flow, this illustration has been included because a similar dike in McRae Canyon may have influenced the location of historic Ojo del Muerto spring (see Figure M-4).



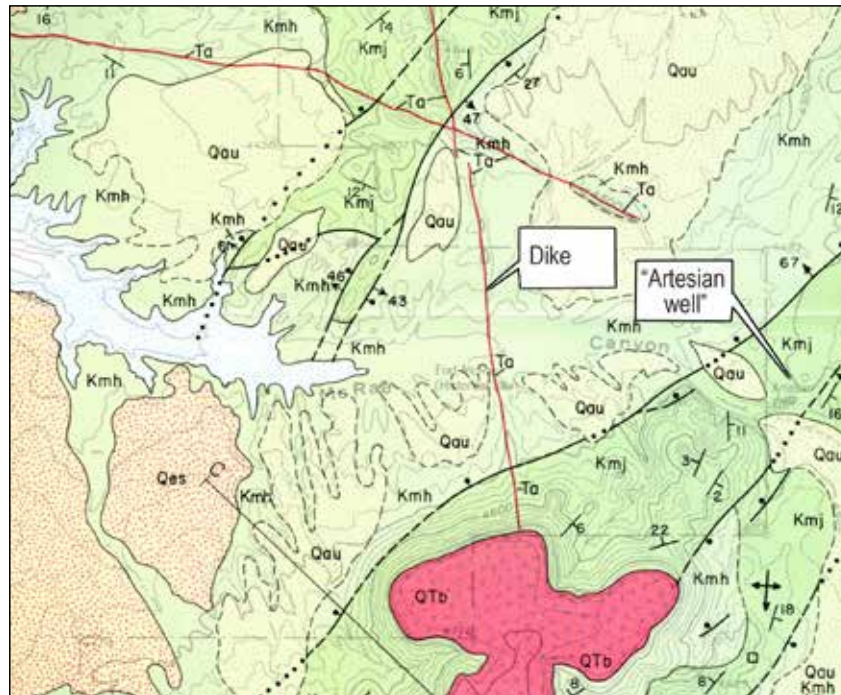


**Figure M-4.** Geologic map showing north-trending andesite dike (Ta; our Ti) crossing McRae Canyon at Fort McRae Historic Site. This map is a portion of the Elephant Butte quadrangle by Lozinsky (1987). The dike crosses faults and intrudes Cretaceous Jose Creek member (Kmj) and Hall Lake member (Kmh) of the McRae Formation (our Bks). Other map symbols include Plio-Pleistocene basalt lava flows (QTb), undifferentiated alluvium (Qau; similar to our Qvo), eolian sand sheets (Qes), and the reservoir level (blue stipples at 4,400 feet elevation). The dike runs just east of Fort McRae and reportedly forced water to the surface at the fort until construction of a reservoir upstream from the Fort by AT&SF Railroad Co. in the 1880s diverted this flow (Department of the Interior, 1893). Note, "Artesian Well" marked on map to the east of Fort McRae is the present location of the Ojo del Muerto spring.



**Figure M-5.** Google Earth™ image showing the remains of Fort McRae in lower left, with dike crossing drainage to east. Where dike crosses the channel is the historic location of the Ojo del Muerto spring. Present location of spring is upstream to the right.





**Figure M-6.** Present location of Ojo del Muerto spring, McRae Canyon. View is downstream along channel. Major outflow from spring enters channel from left in center of photo, just downstream from the larger cottonwood tree on the left bank of the channel.



**Figure M-7.** Sandstone beds exposed as eroded ledges in bottom of McRae Canyon, just upstream from primary outlet of the spring, at the present day location of Ojo del Muerto Spring. X-ray diffraction analysis (XRD) of white evaporate crust seen in photo identified as a combination of thenardite and halite ( $\text{Na}_2\text{SO}_4$ ,  $\text{NaCl}$ ).





**Figure M-8.** Seep in arroyo, near JM-508, McRae Canyon. Photo was taken March, 2014, six months after heavy monsoon rains. The extensive algal growth indicates that water has been present at the surface for a substantial period of time. In addition, the lack of evaporite minerals in the channel indicates that the water is low in dissolved salts, suggesting that the water in the channel is recently derived from rainfall rather than from a deeper subsurface flow path. This intermittent water supply is approximately half way between Ojo del Muerto spring and the large playas near Engle. It extends upstream at least 1.5 km from JM-508.



**Figure M-9.** Ash Canyon Spring (JM-509). This spring lies outside of the project area to the west. At this location, ground water rises to the surface above bedrock. Shallow alluvium discontinuously covers bedrock along the channel length. Numerous such seeps/springs occur along this and neighboring canyons.





**Figure M-10.** Mescal Spring (JM-500) in Mescal Canyon. This spring lies to the west of Ash Spring, and discharges under similar circumstances. Additional seeps/springs are located in this canyon.



**Figure M-11.** Shallow ground water in channel deposits, Aleman Draw seep (JM-506). The arroyo channel consists of shallow sand and gravel over Eocene bedrock (Love Ranch Formation). Location is just downstream from railroad trestle crossing Aleman Draw. Photo (and water sample) were taken October, 2013, one month after major monsoon rainfall.



**Figure M-12.** Hole dug in arroyo channel by animals to access shallow ground water, Yost Draw. Arroyo channel consists of shallow sand/gravel over Eocene bedrock (Love Ranch Formation). Location is east of CR A-13, and south of Aleman Draw.





**Figure M-13.** Collecting water sample from shallow ground water, Yost Draw seep (JM-507). Note evaoporites along capillary fringe in channel alluvium, indicating shallow water table. White powdery crust is made of sulfate evaporites such as gypsum ( $\text{CaSO}_4 \cdot 2\text{H}_2\text{O}$ ), thenardite ( $\text{Na}_2\text{SO}_4$ ), or bloedite ( $\text{Na}_2\text{Mg}(\text{SO}_4)_2 \cdot 4\text{H}_2\text{O}$ ). Depth to water at this location during March 2014 was 15–20 cm. Location is east (downstream) of animal water hole seen in figure M12.



**Figure M-14.** Bifurcating channels on floodplain playa (Qlf) in Jornada Draw northwest of Prisor Hill. Playa is presently dry, but undergoes periodic inundation. Note multiple sets of polygonal cracks forming fissures in the dry clay and rubbly texture of broken clay platelets at the surface of the channels. Tobosa grasses hide uplifted blocks of clay called "gilgai." These features are common in clays that swell when they are wet and shrink when they are dry.





**Figure M-15.** Hand dug concrete lined cistern. Cistern is located in the southern portion of the project area. Shaft is 5 ft wide by 7 ft deep, but may be deeper as base of shaft filled with sediments and debris. Materials excavated during the construction of the cistern were apparently used to create an earthen berm to channel runoff from Barbee Draw into the mouth of cistern. The water was probably used for livestock. While this indicator of surface water is not strictly speaking geological in nature, it does show that periodic sheet wash was frequent enough and substantial enough to induce people to attempt to harvest and store these waters.



**Figure M-16.** Second hand dug concrete lined cistern. Shaft is 4 ft wide by 8 ft deep and excavated into small remnant of Qp2 surface. Shaft may be deeper. As with the cistern described in figure M15, this water feature appears to have been filled with runoff from Barbee Draw.



## Locations with Indicators of Past Shallow Groundwater



**Figure P-17.** Stains and mineral precipitation in late Quaternary alluvium (Qva). Staining indicates higher levels of the water table exposed in an arroyo wall along Cañon del Muerto drainage. Maroon sandstone at base is Cretaceous McRae Formation (Rks). Lower alluvium is pebbly sand with many cross-cutting channels. Rusty brown and dark gray irregular masses of iron and manganese oxides indicate chemical precipitation in past shallow groundwater. Finer-grained alluvium above top of rod is coated with evaporite minerals and calcium carbonate along a subsurface horizon, probably indicating a paleo-capillary zone above the water table. Rod is 1.5 m long, marked in 10 cm increments.



**Figure P-18.** Closer view of stains and cementation in late Quaternary alluvium (Qva). Staining exposed in an arroyo wall along Cañon del Muerto drainage. Rusty brown and dark gray irregular masses and stains of iron and manganese oxides indicate alteration within the saturated zone of past shallow groundwater.





**Figure P-19.** Arroyo cut, McRae Canyon. Multiple levels of iron and manganese oxide coatings are visible in the center of the profile. Lower white evaporite in capillary fringe above bedrock may indicate lateral movement of local groundwater along contact. Closeup of manganese and iron oxide coatings in arroyo cut bank, McRae Canyon.

## Hackberry Draw

**Figure P-20.** Rust and evaporate minerals in lower arroyo wall may indicate shallow groundwater in past. Location is in Hackberry Draw. Shovel handle is 1 m long.

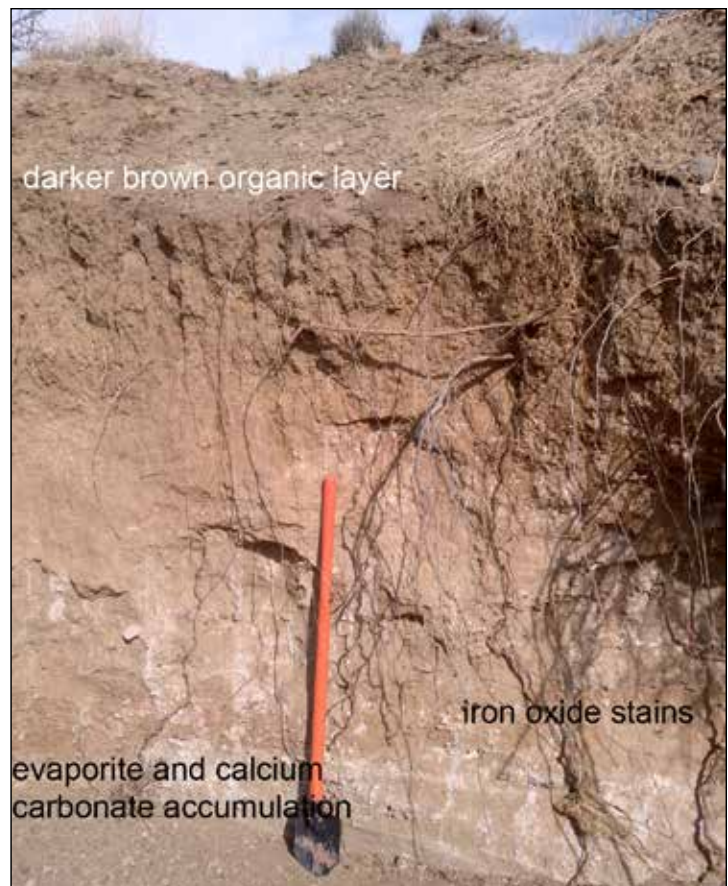






**Figure P-21.** Elevated organic matter exposed in arroyo profile. Pale gray and dark brown horizons at top of shovel handle indicate elevated organic content and may represent zone of wet soils and possibly a shallow groundwater level in the Holocene epoch. Photo was taken in Hackberry Draw.



**Figure P-22.** Fault zone, Aleman Draw. Fault zone with evaporite minerals and calcium carbonate precipitated along fractures in fault zone cutting Cretaceous sedimentary rocks (Rks) in Aleman Draw.



## Aleman Draw

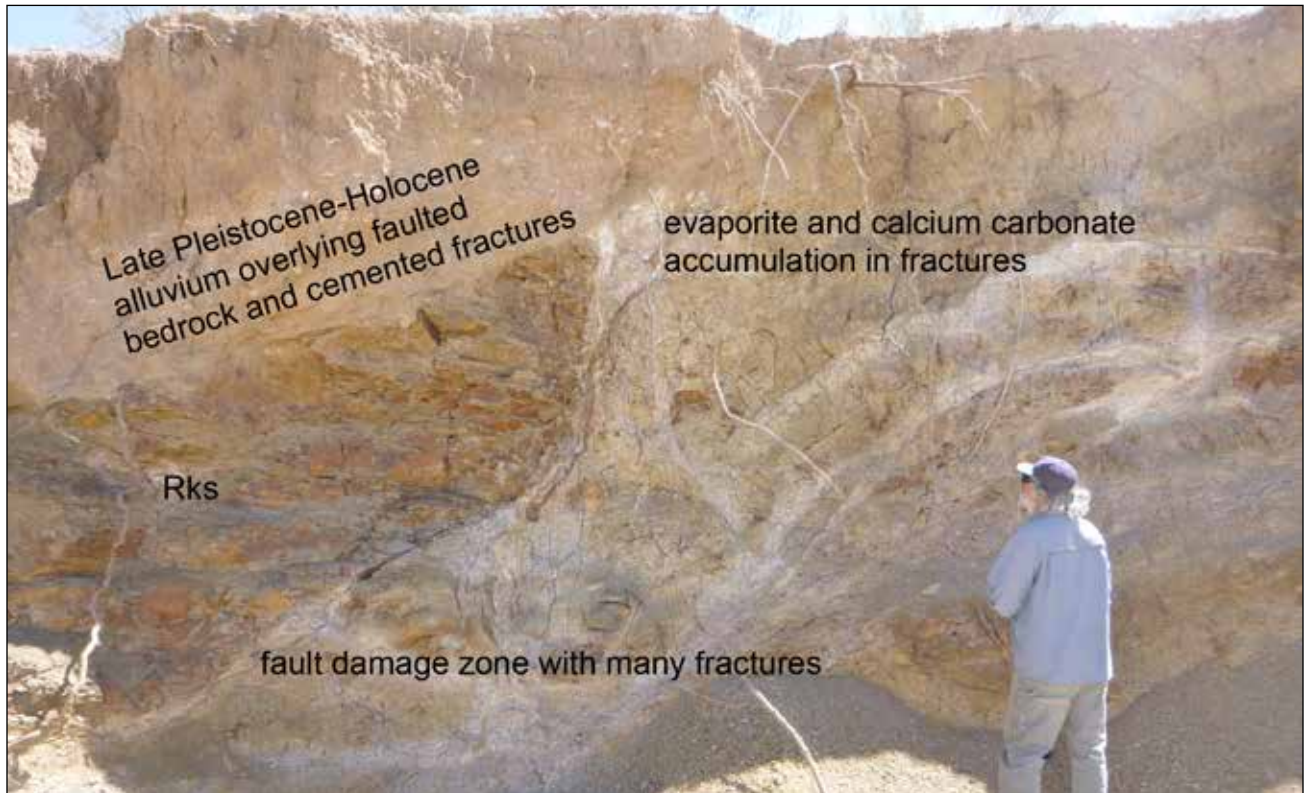


**Figure P-23.** Close up of fault zone with calcium carbonate and evaporite minerals in Aleman Draw. Note Quaternary alluvium on upper left truncates fault and Cretaceous bedrock. Precipitated minerals along the fault zone indicate that groundwater moved along the fractures, although direction of movement has not been determined.



**Figure P-24.** Secondary calcium carbonate precipitation high in arroyo cut bank, near railroad trestle, Aleman Draw. The cemented calcium carbonate indicates elevated groundwater levels in the Pleistocene (>11,000 years ago).





**Figure P-25.** Angular unconformity along Aleman Draw. Angular unconformity between maroon sandstone and mudstone of the Love Ranch Formation (Rts) and overlying late Quaternary alluvium (Qap) along Aleman Draw at Aleman, NM. Note white deposits of evaporite in alluvium above the unconformity, indicating shallow groundwater during the Holocene. Rod is 1.5 m long.

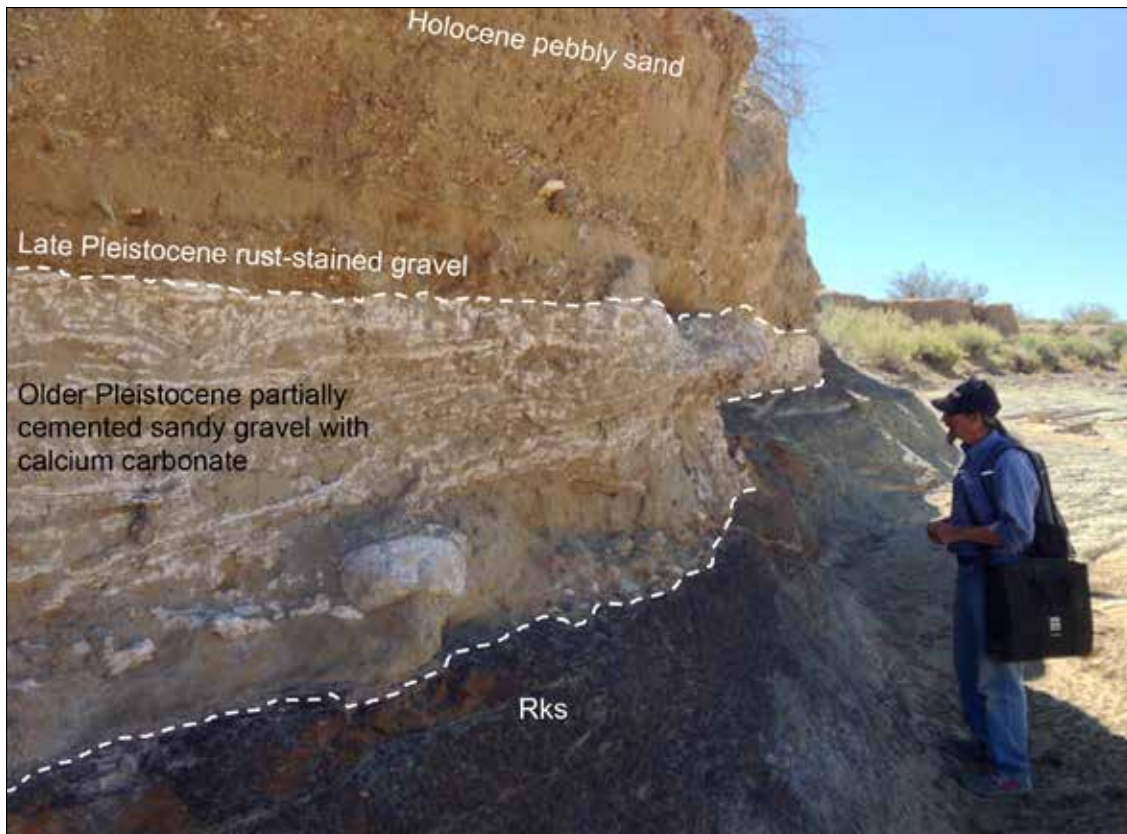


**Figure P-26.** Two unconformities exposed in Aleman Draw. Lower maroon and gray unit is McRae Formation (Rks). The overlying pale tan unit with pebbly base is Quaternary alluvium (older than 100,000 years). Whitish blobs and stringers are calcium carbonate cement showing elevated groundwater levels in the Pleistocene (>11,000 years ago). The uppermost reddish-brown unit with a pebbly base is late Quaternary arroyo alluvium (Qap) with no indication of shallow groundwater.

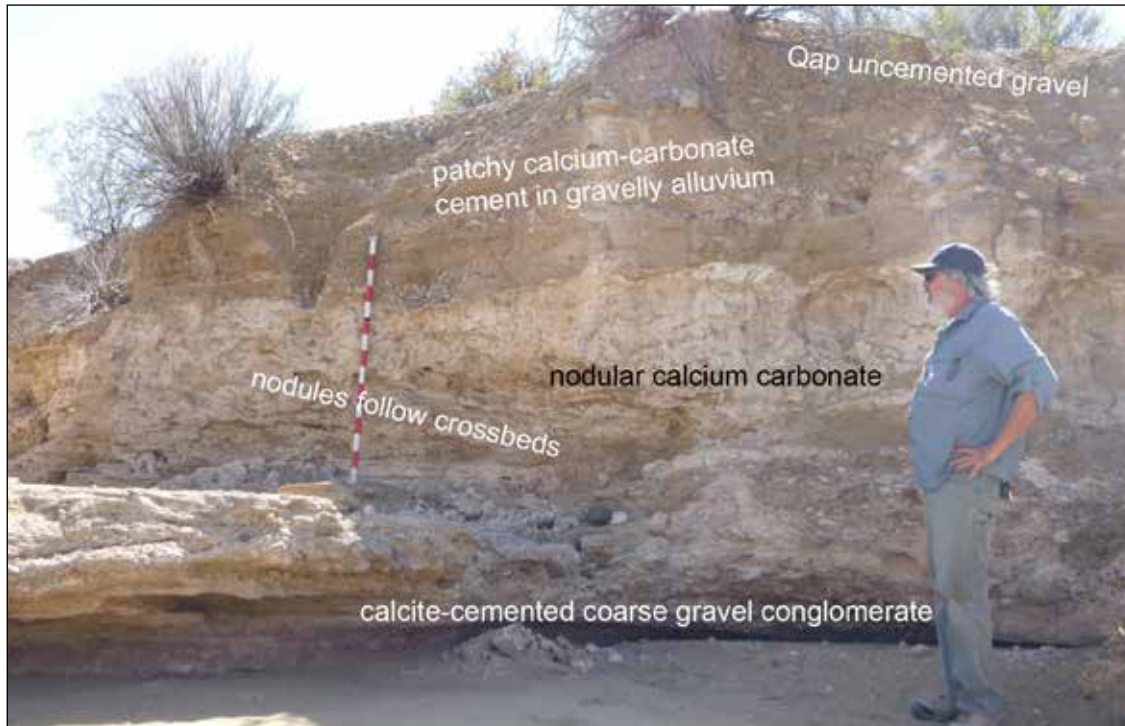


**Figure P-27.** Multiple Pleistocene-age episodes of calcium-carbonate cementation and shallow groundwater-levels revealed in wall of Aleman Draw west of the railroad trestle. Lower coarse gravel and sand are cemented with poikilotopic (coarse crystals) of calcite. Middle unit of white, fine-grained, nodular calcium carbonate may be from a separate episode of growth of nodules in a capillary fringe zone after initial precipitation pedogenically in a soil. Crossbedded sand and gravel above 1.1 m on 1.5 m rod is partially cemented with fine-grained calcium carbonate. Coarse gravelly alluvium (Qap) at top is not cemented nor stained.



**Figure P-28.** Indications of shallow groundwater in the past in exposures along the North Fork of Putnum Draw. Lower half-meter is clayey alluvium with white evaporite minerals and calcium carbonate accumulation indicating shallow groundwater—possibly a wet meadow. Rusty iron-oxide stained alluvium is in contact with the clay and also indicates shallow groundwater during the Holocene. Dark brown alluvium above top of 1.5 m rod indicates a period of soil development before burial by more recent alluvium (Qap).



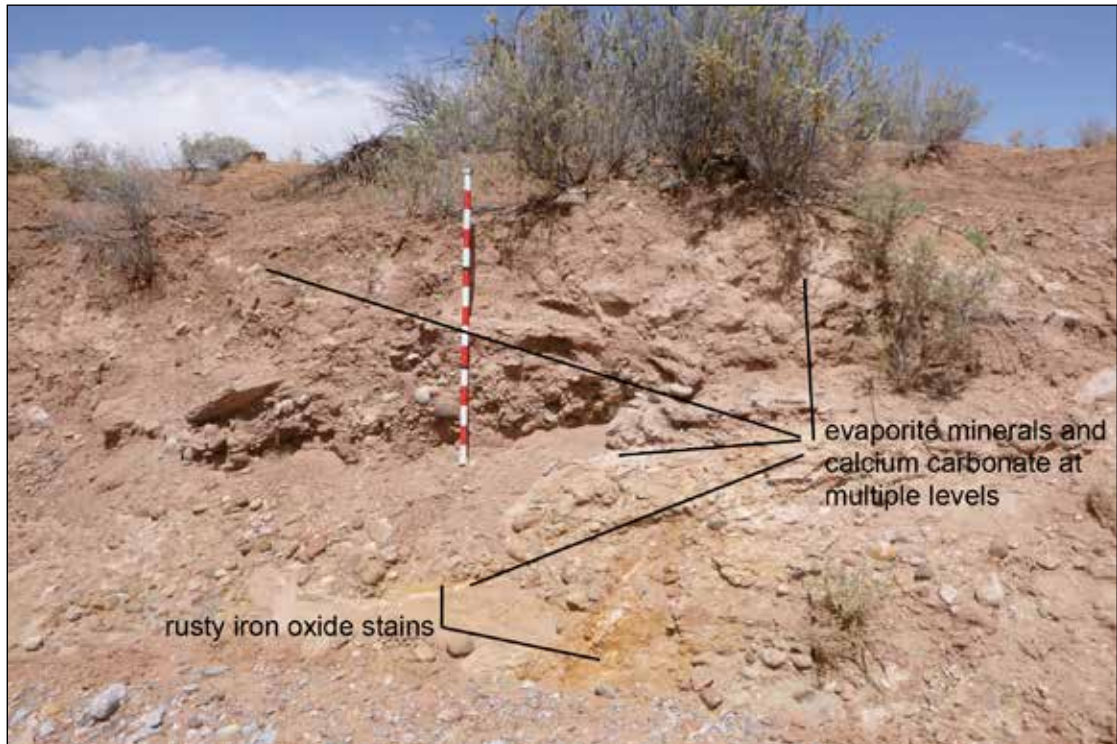


**Figure P-29.** Rust stains (iron oxide) and evaporite minerals exposed in late Quaternary deposits in arroyo wall of Yost Draw. Rusty iron oxide suggests an oxidizing wet environment at the top of a zone of shallow groundwater.

## Yost Draw



**Figure P-30.** Oriented poikilotopic concretions. Concretions found in sandstone cemented along unconformity between maroon Love Ranch Formation (Rts) and Quaternary alluvium (Qap) in Yost Draw. These oriented concretions with macro-calcite indicate subaqueous precipitation of calcium carbonate and the paleo-flow direction (downstream).



**Figure P-31.** Large concretions cemented by calcium carbonate and iron oxides developed in sandstones of the Cretaceous Crevasse Canyon Formation (Rks) probably developed under saturated conditions during late Cretaceous time. The sandstone is also cemented with lesser amounts calcium carbonate and clay.

## References

- Berner, R., 1962a, Stability relations of  $\text{Fe}_2\text{O}_3$ ,  $\text{Fe}_3\text{O}_4$ ,  $\text{FeS}_2$ + $\text{FeCO}_3$  in water at  $25^\circ\text{C} + 1$  atm. total pressure;  $\Sigma\text{CO}_2=10^{-1.5}$ ;  $\Sigma\text{S}=10^{-6}$  solid-ion boundaries at  $10^{-6}$  dissolved Fe, in H. H. Schmitt, ed., *Equilibrium diagrams for minerals at low temperature and pressure*: Cambridge (Massachusetts), Geological Club of Harvard, p 76.
- Berner, R., 1962b, Stability relations of  $\text{FePO}_4 \cdot 2\text{H}_2\text{O}$ ,  $\text{FeSO}_4 \cdot 7\text{H}_2\text{O}$ ,  $\text{Fe}(\text{OH})_3$  + pyrite in water at  $25^\circ\text{C}$ ;  $P_{\text{total}} = 1$  atm;  $\Sigma\text{P}=100$ ;  $\Sigma\text{S}=10^{-4}$ ; solid-ion boundaries at  $10^{-4}$  dissolved Fe, in H. H. Schmitt, ed., *Equilibrium diagrams for minerals at low temperature and pressure*: Cambridge (Massachusetts), Geological Club of Harvard, p 77.
- Birkeland, P. W., Machette, M. N., and Haller, K. M., 1991, *Soils as a tool for applied Quaternary geology*: Utah Geological and Mineral Survey, Miscellaneous Publication 91-3, 63 p.
- Eckstrand, O. R., 1962, Eh-pH diagram showing solid phases in equilibrium with  $\text{H}_2\text{O}$  at  $25^\circ\text{C}$ , 1 atm. total pressure;  $\Sigma\text{CO}_2 = 10^{-4}$ ; and ion fields, in H. H. Schmitt, ed., *Equilibrium diagrams for minerals at low temperature and pressure*: Cambridge (Massachusetts), Geological Club of Harvard, p. 65.
- Gile, L. H., Hawley, J. W. and Grossman, R. B., 1981, *Soils and geomorphology in the Basin Range area of southern New Mexico--guidebook to the Desert Project*: New Mexico Bureau of Mines and Mineral Resources, Memoir 39, 222 p.
- Gile, L. H., Peterson, F. F. and Grossman, R. B., 1966, Morphological and genetic sequences of carbonate accumulation in desert soils: *Soil Science*, v. 101, n. 5, p. 347-360.
- Krauskopf, K. B., 1979, *Introduction to geochemistry*, Second Edition, McGraw-Hill Book Company, New York, 617 p.
- Lozinsky, R. P., 1986, *Geology and Late Cenozoic history of the Elephant Butte area, Sierra County, New Mexico*: New Mexico Bureau of Mines and Mineral Resources, Circular 187, 40 p.
- Monger, H. C., Gile, L. H., Hawley, J. W., and Grossman, R. B., 2009, *The Desert Project—An analysis of arid-land soil-geomorphic processes*: New Mexico State University, Agricultural Experiment Station, Bulletin 798, 76 p.
- Schaetzl, R. J., and Anderson, S., 2005, *Soils: Genesis and Geomorphology*: Cambridge University Press, 817 p.
- Schmitt, H. H., ed., 1962, *Equilibrium diagrams for minerals at low temperature and pressure*: Cambridge (Massachusetts) Geological Club of Harvard, 199 p.
- Smith, H., 1893, Decision of the Hon. Hoki Smith in the "Pedro Armendaris" Grant Case. Legal letter to the Commissioner of the General Land Office on the decision about the location of Ojo del Muerto.





# APPENDIX C

## Model Descriptions

### Playa Modeling

The first model we discuss attempts to simulate the filling and decline of the playas in the area. Four playas; Engle Lake (a) and (b), Jornada Lake, and an unnamed playa, were examined for this study. Landsat imagery, which are satellite photos taken every 16 days, allowed us to create a record of surface area of the playas throughout the past 30 years. This was done by using an area measuring tool to trace the extent of each playa, when they filled, and as they slowly dried up. The satellite imagery showed an interesting phenomenon. We found that, not all of the playas would flood after a large storm event. Sometimes one playa would fill while the others would remain dry, while sometimes the other three would flood, leaving one dry (Figure 1). Several

hypotheses have been proposed to explain this irregularity. As the playas dry, the playa sediments desiccate and create large cracks in the playa bed. These cracks may result in rapid draining of the water. The development of these cracks to varying degrees in different playas may result in varying responses of different playas to the same precipitation regime. A second hypothesis takes localized precipitation into account. Localized summer thunderstorms associated with the North American Monsoon likely result in an uneven spatial distribution of precipitation, causing some playas to fill while others remain dry. To study the playa flooding we used the precipitation record from Elephant Butte, located roughly 15 km away from the playa area. We found that even from this relatively proximal precipitation record, there were occasional flooding events that corresponded

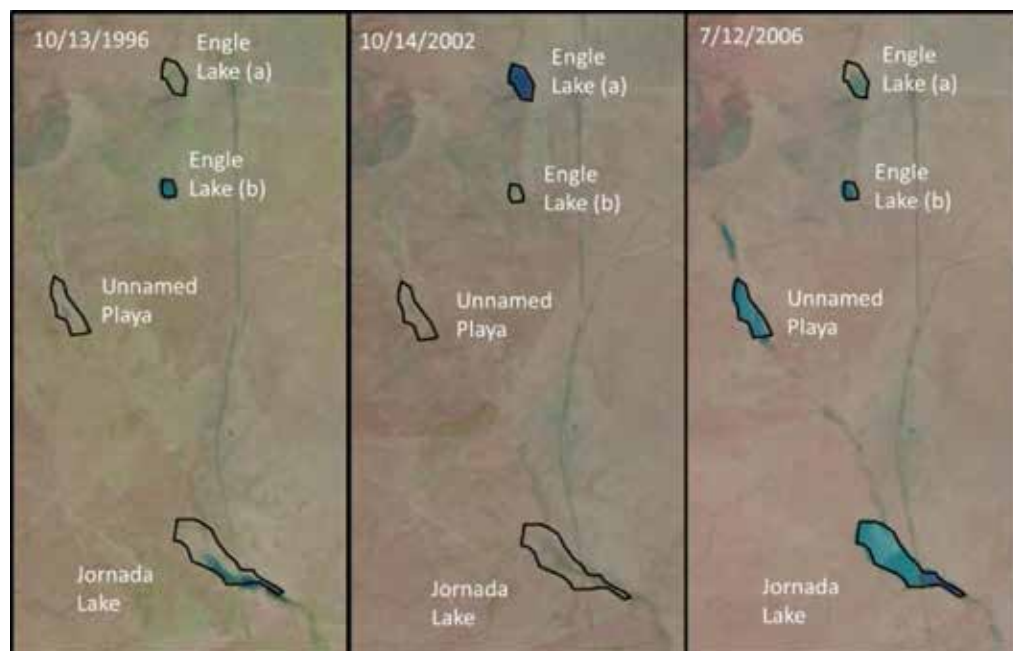


**Figure C-1.** Above are three Landsat captures of the playa region captured after storms in 1996, 2002, and 2006. This figure emphasizes the irregularity of which playas flood following a storm.

with very small storms. To smooth the data for modeling purposes, the four playas areas were treated as a single playa.

Using the temporal record of flooding, as well as the precipitation record collected at Elephant Butte, we filtered the data to find a relationship between the magnitude of storms and the filling of the playas. By matching the record of flooding events with significant storms we found that the best fit threshold for flooding to occur came when more than two inches of rain fell over the period of a week. Next, we fit an exponential regression to match the rate at which the playas dried up following being filled. This takes into account the magnitude of the filling event, matches the observed decline in the area of the playas with time as result of evaporation and surface water infiltration, and predicts how long water remains in the playas (Figure 2).

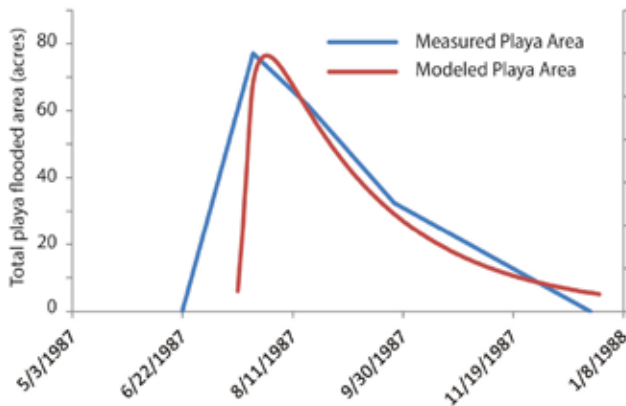


**Figure C-2.** Comparing the measured playa area to the modeled playa area.

## Modeling of springs

Two rudimentary 1D Boussinesq groundwater flow models were constructed in Excel to estimate discharge at the springs, assuming saturated, horizontal flow through a homogeneous aquifer. One model describes the local springs and seeps, and the other models the regional spring, Ojo del Muerto. There are several inputs for each model we had to estimate; these include hydraulic conductivity ( $K$ ), gradient length the aquifer flow path ( $x$ ), location of recharge, and the amount of recharge infiltrating to the aquifer ( $R$ ). In a confined case specific yield ( $b/x$ ) and aquifer thickness ( $b$ ) are used.

$$\frac{\partial^2 h}{\partial x^2} = \frac{S_y}{Kb} \frac{\partial h}{\partial t} + R$$

## Local Springs and Seeps Modeling

We assume the water discharging at the local springs and seeps originates within the individual watersheds, up gradient of the water source. This assumption is based on the groundwater age (Figure 26), and water chemistry (Figure 24) of the discharging water (OFR 573, page 31). As result, we determined the recharge mechanism for these water sources originates as overland runoff, from large storms. The modeled flow path runs parallel to the stream, where these springs and seeps occur. This means the location of recharge is assumed to cover the entire model. As runoff is the primary water source for the model we determined the 'length of the aquifer' by finding the average distance to the boundary of the watershed from the discharge point, which is approximately 4 km (2.5 mi). The watersheds for the springs and seeps were delineated using the Spatial Analyst toolbox in ArcGIS.

To determine available recharge, runoff calculations for this region were used to estimate the minimum rainfall required to create overland flow. Using these equations, we can estimate when runoff is likely to occur due to excess precipitation (developed by the USDA Natural Resources Conservation Service). Runoff calculation equations are:

$$Q = \frac{(P - 0.2S)^2}{(P + 0.8S)}$$

$$S = \frac{1000}{CN} - 10$$

Where  $Q$  is the runoff,  $P$  is rainfall,  $S$  is the potential maximum retention after runoff begins, and  $CN$  is the curve number which is determined by the USDA, and that takes into account vegetation type, and land slope.

Using this method we found storms producing more than and 0.97 inches of rain result in runoff. As result, we filtered the precipitation data for storms that met or exceeded this threshold. In the southwest, approximately 5% of runoff is estimated to recharge the shallow aquifers (Wilson and Guan, 2004). The final recharge value that is entered into the model throughout the modeled domain is 5% of the precipitation produced by storms large enough to result in runoff ( $>0.97$  in). The gradient of the system was found by taking the difference between the highest elevations in the watershed and the elevation of the spring, and dividing by the aquifer length. Hydraulic conductivity is calibrated to be roughly 16 m/day as the sediment is a highly conductive sand and gravel



alluvium. The model solves for head along a transect of the drainage basin each day throughout the entire period which we have precipitation data. The boundary conditions on either side of this 1D model are fixed head.

## Regional Spring Modeling

The Ojo del Muerto spring is thought to have a very different recharge mechanism. The age of the groundwater and the water chemistry tells us that the water discharging at the spring entered the aquifer approximately 11,000 years ago. This tells us that the flow path which supplies water to the spring is very long and isolated from the surface runoff. Based on water chemistry analyses we determined that chemical signature of the spring matches other wells in the area that tap the McRae aquifer (Geohydrology Associates, 1989). Using geologic cross sections, and the water table map we look for areas where the McRae aquifer is not confined, or sections which would allow infiltration through the impermeable layers above it. We determined that the most likely location for groundwater to recharge this system is from the playa lakes.

With this information another Boussinesq model was constructed, which models the head along a profile from the playas and spring (Figure 30, OFR

573, page 38). The length of the aquifer flow path being modeled is the distance between the playas and the discharge point, 9 km. The gradient of the model was found using the difference in elevation at the playas and the spring, divided by the aquifer length. Recharge to the model occurs only at the playas so only one cell on the edge of the model receives recharge. Because we assume that the recharge to the spring is the result of infiltration from the playa lakes we use the model that estimated when the playas were full to account for recharge. For recharge to occur the water must infiltrate through the playa sediments, which generally have very low conductivity values (~0.01 m/d). As result, when the playas are full, 0.01 m/d of recharge is assigned to the model. Even with very low values, significant volumes of water can infiltrate creating very steady sources of recharge when the playas are flooded in this otherwise dry environment.

Next, we estimated the hydraulic conductivity value for the aquifer by using the travel time water takes to move from the recharge location, to the spring (11,000 years, based on uncorrected C14 dates). The estimated hydraulic conductivity was 1 m/day. This agrees with hydraulic conductivity tests conducted in the McRae which range from 0.5 to 1.7 m/day (Geohydrology Associates, 1989). The boundary conditions on either side of this 2D model are fixed head, playa elevation, and spring elevation.

## References

- Geohydrology Associates, Inc., 1989. Assessment of Geohydrologic Conditions and the Potential for Ground-Water Development in the McRae Aquifer System, Sierra County, New Mexico. Consultant's Report prepared for Oppenheimer Industries.
- Wilson, J.L., Guan, H., 2004, Mountain-block hydrology and mountain-front recharge: Water Science and Application, 9, 113-137.



New Mexico Bureau of Geology and Mineral Resources

A division of New Mexico Institute of Mining and Technology

Socorro, NM 87801

(575) 835 5490

Fax (575) 835 6333

[geoinfo.nmt.edu](http://geoinfo.nmt.edu)